

Lawrence Berkeley National Laboratory

LBL Publications

Title

Physically and chemically smooth cesium-antimonide photocathodes on single crystal strontium titanate substrates

Permalink

<https://escholarship.org/uc/item/0vh2z7t6>

Journal

Applied Physics Letters, 120(19)

ISSN

0003-6951

Authors

Saha, Pallavi
Chubenko, Oksana
Gevorkyan, Gevork S
[et al.](#)

Publication Date

2022-05-09

DOI

10.1063/5.0088306

Copyright Information

This work is made available under the terms of a Creative Commons Attribution-NonCommercial License, available at <https://creativecommons.org/licenses/by-nc/4.0/>

Peer reviewed

Authors to whom correspondence should be addressed: [Pallavi Saha, psaha6@asu.edu; Siddharth Karkare, karkare@asu.edu]

Physically and Chemically Smooth Cesium-Antimonide Photocathodes on Single Crystal Strontium Titanate Substrates

Pallavi Saha,¹ Oksana Chubenko,¹ Gevork S. Gevorkyan,¹ Alimohammed Kachwala,¹ Christopher J. Knill,¹ Carlos Sarabia-Cardenas,¹ Eric Montgomery,² Shashi Poddar,² Joshua T. Paul,³ Richard G. Hennig,⁴ Howard A. Padmore,⁵ and Siddharth Karkare¹

¹Department of Physics, Arizona State University, Tempe, AZ 85287, USA

²Euclid Beamlabs, LLC, Bolingbrook, IL 60440, USA

³Argonne National Laboratory, Lemont, IL 60439, USA

⁴University of Florida, Gainesville, FL 32611, USA

⁵Lawrence Berkeley National Laboratory, Berkeley, CA 94720, USA

(*Electronic mail: karkare@asu.edu)

(*Electronic mail: psaha6@asu.edu)

(Dated: 22 April 2022)

The performance of X-ray Free Electron Lasers and Ultrafast Electron Diffraction experiments is largely dependent on the brightness of the electron sources from photoinjectors. The maximum brightness from photoinjectors at a particular accelerating gradient is limited by the Mean Transverse Energy (MTE) of the electrons emitted from the photocathodes. For high Quantum Efficiency (QE) cathodes like alkali-antimonide thin films, which are essential to mitigate the effects of non-linear photoemission on MTE, the smallest possible MTE and hence the highest possible brightness is limited by the nanoscale surface roughness and chemical inhomogeneity. In this work, we show that high QE Cs₃Sb films grown on lattice-matched Strontium Titanate (STO) substrates have a factor of 4 smoother, chemically uniform surfaces compared to those traditionally grown on disordered Si surfaces. We perform simulations to calculate roughness induced MTE based on the measured topographical and surface-potential variations on the Cs₃Sb films grown on STO and show that these variations are small enough to have no consequential impact on the MTE and hence the brightness.

The brightness of electron beams is a key figure of merit for state-of-the-art ultrafast science tools such as X-ray Free Electron Lasers (XFELs) and Ultrafast Electron Diffraction/ Microscopy (UED/UEM) experiments. An increase in the electron beam brightness can lead to generation of higher power and shorter wavelength x-ray pulses in existing XFELs¹ as well as enable the development of compact XFELs². From the perspective of UED applications, higher beam brightness will cause an increase in the spatio-temporal resolution and allow study of crystals with larger lattice sizes, enabling ground-breaking research in the ultrafast study of quantum materials and critical chemical and biological processes³.

High density bunched electron beams for the above applications are typically produced using photoinjectors which consist of a photoemissive surface (photocathode) placed in an accelerating electric field (E) along with electron optics to mitigate the brightness-degrading effects of space charge. The accelerating electric field is typically in the range of a few to 100 MV/m depending on the design of the photoinjector and the required application⁴.

For most photoinjectors the maximum achievable brightness scales according to the following relation:

$$B \propto \frac{E^n}{\text{MTE}}, \quad (1)$$

where n is a real number between 1 and 2 depending on the design of the photoinjector and MTE is the mean transverse energy of the electrons emitted from the photocathode.

The Mean Transverse Energy (MTE) can be related to the

normalized transverse emittance $\varepsilon_{n,x}$ from the photocathode via the relation:

$$\varepsilon_{n,x} = \sigma_x \sqrt{\frac{\text{MTE}}{mc^2}}, \quad (2)$$

where σ_x is the rms size of the emission area on the cathode, m is the rest mass of a free electron and c is the speed of light.

Typically, the maximum possible accelerating electric field is set by the design of the photoinjector, however, the MTE is a function of the photocathode material, its surface and the photon energy used for emission. Hence minimizing the MTE from photocathodes is critical for maximizing the electron beam brightness from photoinjectors. For a typical bunch charge, the smallest possible MTE (and hence highest brightness) is limited to a few meV due to point-to-point electron interactions⁵ and disorder induced heating of the electron bunch⁶.

The MTE from the cathode is typically proportional to one third of the excess energy (energy difference between the incident photon energy and the work function of the cathode surface)⁷. However, for low or negative excess energy the MTE becomes limited by the Fermi tail of the electron distribution to $k_B T$, where k_B is the Boltzmann constant and T is the lattice temperature of the cathode⁸. This thermal limit has been experimentally demonstrated for thin polycrystalline Sb films at room temperatures resulting in an MTE of 25 meV⁹. Reduction in MTE down to 5 meV from the Cu(100) surface cooled to cryogenic temperatures has also been demonstrated¹⁰. However, such metal cathodes have an

This is the author's peer reviewed, accepted manuscript. However, the online version of record will be different from this version once it has been copyedited and typeset.

PLEASE CITE THIS ARTICLE AS DOI: 10.1063/5.0088306

extremely low Quantum Efficiency (QE), typically less than 10^{-6} - 10^{-8} at threshold photon energies. Hence, a large laser fluence is required to extract the charge densities required for the various XFEL and UED photoinjector applications. The large laser fluence conditions result in MTE of few 100 meV due to non-linear photoemission effects of laser heating¹¹ and multiphoton emission^{12,13}.

One way to mitigate the MTE-degrading effects of non-linear photoemission is to use high-QE, low-electron-affinity semiconductor cathodes like alkali-antimonides. Such cathodes don't require very large laser fluence to attain the required charge densities. Alkali-antimonides like Na_2KSb , K_2CsSb and Cs_3Sb have already been successfully used in photoinjectors to achieve very high average beam currents approaching 100 mA due to their very high quantum efficiency (>1%) in visible (green) light for energy recovery linac applications¹⁴⁻¹⁶. The MTE and QE performance of Cs_3Sb close to the photoemission threshold (wavelength range of 600 nm - 700 nm) has also been investigated at both room and cryogenic temperatures, with the goal of minimizing the MTE¹⁷ and achieving the highest possible brightness in photoinjectors. The smallest MTE measured from Cs_3Sb films was 40 meV at room temperatures and 22 meV at 90 K - significantly larger than the thermal limit of 25 meV at room temperature and 8 meV at 90 K¹⁷. This MTE above the thermal limit was attributed to the non-uniform nature of the Cs_3Sb surface. These measurements were performed at low electric fields well below 1 MV/m. Hence it is critical to produce alkali-antimonide films with minimal surface non-uniformities to maximize the brightness of electron beams.

Surface non-uniformities such as physical roughness and work function variations (often termed chemical roughness) can result in transverse accelerating fields close to the cathode surface increasing the MTE in photoinjectors. Nano-scale physical roughness on the cathode surface bends the accelerating electric field lines close to the surface resulting in transverse acceleration of the emitted electrons increasing the MTE. The resulting MTE increase is proportional to the accelerating electric field, the square of the amplitude of the roughness and inversely to the periodicity¹⁸. Chemical roughness on the other hand produces transverse electric fields between regions with varying work functions. These electric fields also result in increased MTE, however, their effect on MTE reduces with increasing accelerating electric field¹⁹. The combined effects of physical and chemical roughness from realistic cathode surfaces on MTE can result in a non-trivial, non-monotonic dependence of MTE on the accelerating electric field. This dependence can be obtained computationally by using a Fourier-like decomposition of the resultant electric field close to the surface and numerically tracking the trajectories of electrons in this field²⁰.

In order to minimize the effects of physical and chemical roughness on MTE, there has been a considerable effort undertaken to develop alkali-antimonide thin film growth techniques that result in minimal surface non-uniformities. The films that are grown using the traditional sequential process of first depositing several nm thick Sb film followed by the deposition of alkali metals at elevated temperatures results

in a large roughness exceeding several nm rms with a spatial period of 100 nm²¹. Such films often result in unacceptably large roughness induced MTEs. A significantly smoother surface of alkali-antimonide films (with 0.6 nm rms roughness) was achieved by co-depositing the Sb and alkali-metals onto a Si substrate at elevated temperatures¹⁸. The MTE increase per unit accelerating electric field $\Delta\text{MTE}/E = 0.5$ meV/(MV/m) due to the physical roughness was computed from the atomic force microscopy (AFM) measurements on such surfaces. Co-deposition of Cs and Sb on single crystal substrates like 3C-SiC (100), $\text{Al}_2\text{O}_3(10\bar{1}0)$, $\text{TiO}_2(001)$ that are lattice matched to Cs_3Sb , was investigated as a route toward achieving smoother, ordered surfaces of Cs_3Sb with reduced MTE²². Among these lattice-matched substrates, 3C-SiC(100) resulted in the smallest physical roughness with $\Delta\text{MTE}/E$ ranging between 0.24-0.79 meV per MV/m. Even in the best case scenario of 0.24 meV/(MV/m) the MTE increase due to physical roughness at large accelerating gradients of 100 MV/m is comparable to that of the thermal MTE ($k_B T$) at room temperature and significantly exceeds it at cryogenic temperatures.

Despite the significant reduction in surface roughness of alkali-antimonide films, as stated above, the smoothest surfaces achieved will still result in non-negligible contribution to MTE at very large accelerating gradients when trying to achieve the smallest possible MTE. Moreover, the chemical roughness or work function variations on such alkali-antimonide films have not been measured in a reliable fashion. Such variations could dominate the roughness effect on MTE at smaller accelerating fields of < 20 MV/m and could explain the higher-than-thermal MTE measurements from Cs_3Sb at low electric fields¹⁷.

In this paper we present the growth of Cs_3Sb cathodes on the lattice matched ordered (100) surface of Strontium Titanate (STO). We perform simultaneous Atomic Force Microscope (AFM) and Kelvin Probe Force Microscopy (KPFM) measurements to obtain detailed nanoscale physical and chemical roughness maps of the surface of these Cs_3Sb films. We compute the effects of this measured physical and chemical roughness on MTE. Our results show that the Cs_3Sb films grown on STO have a less than 1 meV impact on MTE for a wide range of electric fields up to 100 MV/m, making the issue of surface roughness induced MTE from alkali-antimonides inconsequential for electron beam brightness in any photoinjector even at cryogenic temperatures.

STO(100) was chosen from an open-source list of 150 commercially available candidate substrates²³, which are lattice-matched to Cs_3Sb using the MPIInterfaces software package²⁴. The (100) face of STO (lattice constant 3.93Å) was found to have a 0.7% lattice mis-match with Cs_3Sb (lattice constant 9.334Å), with 3 unit cells of STO corresponding to 1 cubic unit cell of Cs_3Sb . Growth performed on a lattice matched surface could result in epitaxy with higher degree of crystallinity and thus may result in smoother films compared to those grown on disordered/non-lattice-matched substrates like Si or polished metals as demonstrated in this paper.

Cs_3Sb films were grown on both STO and Si substrates. Both STO and Si substrates were purchased from MTI Corp²⁵

This is the author's peer reviewed, accepted manuscript. However, the online version of record will be different from this version once it has been copyedited and typeset.

PLEASE CITE THIS ARTICLE AS DOI: 10.1063/1.50088306

and were atomically-flat, single-crystal, epi-ready substrates with a dis-ordered native oxide formed on the surface. The STO substrate was p-doped with Nb dopants to a value of 0.05% by atomic weight, while the Si substrate was p-doped with boron atoms. Both STO and Si substrates were rinsed with isopropanol and annealed at 600 °C for two hours in an ultra-high-vacuum (UHV) growth chamber¹⁸ with a base pressure in the low 10^{-10} Torr range as is typically done prior to alkali-antimonide growth. For STO, this resulted in a well ordered, atomically smooth, pristine surface, that was confirmed by observing atomic steps/terraces with rms roughness of <0.1 nm using the AFM. For Si, annealing at this temperature gives rise to an atomically smooth, but disordered surface with the native oxide layers and a AFM measured rms roughness of <0.3 nm.

Cs₃Sb thin films were grown via co-deposition of Cs and Sb onto the substrates. During growth, the substrates were heated radiatively and held at a constant temperature of 75 °C. Sb was evaporated by heating 99.9999% pure Sb pellets (Alfa Aesar)²⁶ and Cs was evaporated by heating cesium molybdate pellets (SAES Getters)²⁷, placed in their respective effusion cells²⁸. The Sb source is heated to 400 °C, which corresponds to a flux rate of 0.001 nm/s at the location of the substrate. This flux rate was pre-calibrated using a quartz crystal balance. Cs source temperature was set in the range of 350-450 °C, and was adjusted by a few degrees during the growth to maintain a constant Cs partial pressure of $(1.2 \pm 0.1) \times 10^{-10}$ torr, on a residual gas analyzer (RGA). The Cs source is located 4 inches away from the substrate while the RGA was located in the growth chamber, but out of the direct line of sight of the Cs source.

During deposition the growth was monitored by measuring the QE of the film under illumination with a 532 nm CW laser. The substrates were held at a -30 V bias w.r.t the chamber walls and the current emitted from the substrate was measured using a picoammeter. Growth on both substrates was performed until the QE plateaued. At this point the samples were allowed to cool to room temperature. All the films yielded a high final QE between 2-5 % in the green, as typically expected from Cs₃Sb cathodes.

The QE plateau on the STO substrate was attained within a very short time period of ~15 min from the start of the deposition, while the films on Si typically took ~1.5 hours to plateau. Given the Sb deposition rate of 0.001 nm/s and a factor of 7 higher thickness of the Cs₃Sb film compared to the Sb film thickness²⁹, the 15 min growth on STO corresponds to a very thin film of 6.3 nm and the film on the Si substrate was estimated to be ~40 nm thick. In order to compare the properties of films of equal thickness on the two substrates, a thick film was intentionally grown on the STO substrate as well. Although the QE plateaued on the STO substrate in ~15 min, growth was continued for ~1.5 hours to reach a thickness of ~40 nm, comparable to that of Si. During this period, the QE was largely constant and increased very slowly to a value of ~5%.

Such thin (6.3 nm) films of Cs₃Sb with a QE>2% in the green are atypical. However, recent results of epitaxially grown single crystalline Cs₃Sb films on 3C-SiC (001) have

demonstrated such low-thickness-high-QE behavior³⁰.

The QE spectral response and surface non-uniformities (physical and chemical roughness) of the films were investigated. The QE spectral response was measured by monitoring the photocurrent emitted by the sample using a lock-in amplifier, while light from a pulsed Optical Parametric Amplifier (Light Conversion Orpheus pumped by Light Conversion Pharos) was incident on the sample surface. The fluence of the laser pulses incident on the sample was kept small enough to ensure linear photocurrent to avoid effects of space charge and non-linear photoemission. The physical and chemical roughness was measured using a UHV RHK-AFM instrument connected in UHV to the growth chamber. AFM-KPFM measurements are performed on the samples grown, in the frequency modulation mode by using Si tips coated with Cr/Pt suited for electrical measurements like KPFM³¹. For the AFM measurements, the tip images the sample line by line via raster scanning the sample surface (x,y), while the frequency regulation feedback system maintains a constant frequency shift from the resonance by adjusting the tip-sample distance. The z-motion of the tip to maintain constant frequency shift is the measure of the physical roughness of the sample³². The force between the tip and the sample goes to a minimum when the electrical potential difference applied between them is equal to the contact potential difference. The contact potential difference (relative work function) between the sample and the conducting tip is measured by adding a small voltage oscillation to the sample bias and running a separate feedback loop to keep the force to a minimum during the AFM scan³². The electrical potential difference applied at each point during the raster then gives the KPFM image of the surface contact potential variation or the work function variation. Due to the larger height variations on the film on the Si substrate and the volatile nature of Cs₃Sb, it was not possible to obtain a reliable KPFM image. However, a very clear KPFM image of the films on STO substrate was obtained.

FIG. 1. QE spectral response measured from Cs₃Sb photocathodes grown on STO and Si substrates.

The QE spectral response of the films is shown in figure 1. The cathodes grown on different substrates exhibit similar profiles, QE ranging between 2-5 % in green light and a photoemission threshold near ~ 2.1 eV as indicated by the knee in the spectral response curve.

FIG. 2. 3D topography images of (a) thin Cs₃Sb film on STO, (b) thick Cs₃Sb film on STO and, (c) Cs₃Sb film on Si.

FIG. 3. 3D chemical potential maps of (a) thin Cs₃Sb film on STO and, (b) thick Cs₃Sb film on STO.

Fig. 2 shows the AFM images of the thin film (Fig. 2(a)), thick film (Fig. 2(b)) grown on STO and the film (Fig. 2(c)) grown on Si. Fig. 3 shows the KPFM images obtained on the

thin film (Fig. 3(a)) and the thick film (Fig. 3(b)) on the STO substrate. The KPFM images are taken during the AFM scan and hence represent the exact same area of the film surface.

The thin film on STO has the smallest out-of-plane rms surface roughness of 0.3 nm with an in-plane periodicity ~ 60 nm and a rms surface potential variation (chemical roughness) of 2.65 mV. The thick film on STO has a larger out-of-plane rms surface roughness of 0.6 nm with a larger in-plane periodicity ~ 100 nm and a rms surface potential variation of 4.32 mV. The film on Si has a significantly larger out-of-plane rms surface roughness of 1.4 nm (4 times larger than that of the thin film on STO) with a periodicity ~ 100 nm. The error associated with physical and chemical roughness measurements due to instrumental uncertainty has been estimated to be $\sim 10\%$.

In order to estimate the effects of these measured physical and chemical roughness on the MTE, the electric field close to the surface was calculated using a Fourier-like decomposition for various accelerating gradients. For the Si surface the surface potential variation was assumed to be zero as this data is unavailable. The calculated electric fields closely represent the resultant fields at the actual surface due to the physical roughness, chemical roughness and the accelerating gradient. Electrons with zero initial velocity were launched from various points on the surface. Their motion was tracked in the calculated electric fields until a point sufficiently far away from the surface where the roughness-induced transverse fields become negligible. The rms of the transverse velocities gained by these electrons was used to estimate the roughness-induced MTE increase. The details of this calculation are provided elsewhere²⁰.

Fig. 4 shows this calculated roughness-induced MTE for the 3 surfaces measured at various accelerating gradients. For the film of Si, the roughness induced MTE starts from near 0 at very low electric fields and increases rapidly at larger gradients. At 100 MV/m (typically the maximum accelerating gradient used in photoinjectors) the roughness induced MTE is 40 meV ($\Delta\text{MTE}/E = 0.4$ meV/(MV/m)). The zero roughness induced MTE at low fields is due to the uniform surface potential assumption for the films on Si. In reality, we expect the low-accelerating-gradient-roughness-induced MTE to be larger due to variations in the surface potential (chemical roughness). The MTE increase calculations performed for the films on STO include effects of both physical and chemical roughness. The thick film on STO is significantly smoother giving an MTE increase of only 8 meV at 100 MV/m (dominated by physical roughness) and only 2.2 meV at low gradients (dominated by chemical roughness). Finally, the thin film on STO is smoothest and gives roughness induced MTE smaller than 1 meV at all gradients.

FIG. 4. Effect of surface roughness on MTE. The calculations for the film on Si include effects of physical roughness only.

In conclusion, we have demonstrated the growth of high QE, topographically ultra-smooth and chemically homogeneous Cs₃Sb cathodes on lattice-matched STO substrates. Our results show that the films grown on STO exhibit sufficiently small physical and chemical roughness to make the roughness

induced MTE increase inconsequential at all commonly-used field gradients in photoinjectors.

This work was supported by the U.S. National Science Foundation under Award No. PHY-1549132 - the Center for Bright Beams, the DOE under Grant No. DE-SC0021092, and Grant No. DE-SC0020575. P. Saha and O. Chubenko contributed equally to this work.

- ¹M. Ferrario, "Overview of fel injectors," Proc. of EPAC, Edinburgh, Scotland (2015).
- ²J. B. Rosenzweig, N. Majernik, R. R. Robles, G. Andonian, O. Camacho, A. Fukasawa, A. Kogar, G. Lawler, J. Miao, P. Musumeci, B. Naranjo, Y. Sakai, R. Candler, B. Pound, C. Pellegrini, C. Emma, A. Halavanau, J. Hastings, Z. Li, M. Nasr, S. Tantawi, P. Anisimov, B. Carlsten, F. Krawczyk, E. Simakov, L. Faillace, M. Ferrario, B. Spataro, S. Karkare, J. M. Maxson, Y. Ma, J. Wurtele, A. Murokh, A. Zholents, A. Cianchi, D. Cocco, and S. B. van der Geer, "An ultra-compact x-ray free-electron laser," *New J. Phys.* **22**, 093067 (2020).
- ³P. Musumeci, J. T. Moody, C. Scoby, M. S. Gutierrez, H. A. Bender, and N. S. Wilcox, "High quality single shot diffraction patterns using ultrashort megaelectron volt electron beams from a radio frequency photoinjector," *Rev. Sci. Instrum.* **81**, 013306 (2010).
- ⁴P. Musumeci, J. G. Navarro, J. B. Rosenzweig, L. Cultrera, I. V. Bazarov, J. M. Maxson, S. Karkare, and H. A. Padmore, "Advances in bright electron sources," *Nucl. Instrum. Meth. A.* **907**, 209 (2018).
- ⁵M. Gordon, S. B. van der Geer, J. M. Maxson, and Y. K. Kim, "Point-to-point coulomb effects in high brightness photoelectron beam lines for ultrafast electron diffraction," *Phys. Rev. Accel. Beams.* **24**, 084202 (2021).
- ⁶J. M. Maxson, I. V. Bazarov, W. Wan, H. A. Padmore, and C. E. Coleman-Smith, "Fundamental photoemission brightness limit from disorder induced heating," *Phys. Rev. Accel. Beams.* **15**, 103024 (2013).
- ⁷D. H. Dowell and J. F. Schmerge, "Quantum efficiency and thermal emittance of metal photocathodes," *Phys. Rev. ST Accel. Beams.* **12**, 074201 (2009).
- ⁸T. Vecchione, D. H. Dowell, W. Wan, J. Feng, and H. Padmore, "Quantum efficiency and transverse momentum from metals," *Proceedings of FEL 2013* (2013).
- ⁹J. Feng, J. Nasiatka, W. Wan, S. Karkare, J. Smedley, and H. A. Padmore, "Thermal limit to the intrinsic emittance from metal photocathodes," *Appl. Phys. Lett.* **107**, 134101 (2015).
- ¹⁰S. Karkare, G. Adhikari, W. A. Schroeder, J. K. Nangoi, T. Arias, J. M. Maxson, and H. A. Padmore, "Ultracold electrons via near-threshold photoemission from single-crystal cu(100)," *Phys. Rev. Lett.* **125**, 054801 (2020).
- ¹¹J. M. Maxson, P. Musumeci, L. Cultrera, S. Karkare, and H. A. Padmore, "Ultrafast laser pulse heating of metallic photocathodes and its contribution to intrinsic emittance," *Nucl. Instrum. Methods Phys. Res., Sect. A* **865**, 99 (2017).
- ¹²J. Bae, L. Cultrera, I. V. Bazarov, J. M. Maxson, S. Karkare, H. A. Padmore, P. Musumeci, and X. L. Shen, "Multi-photon photoemission and ultrafast electron heating in cu photocathodes," *Proceedings of the 9th International Particle Accelerator Conference, Vancouver, BC* (2018) paper TUPML026 (2018).
- ¹³C. J. Knill, H. A. Padmore, and S. Karkare, "Near-threshold nonlinear photoemission from cu(100)," *Proceedings of the 9th International Particle Accelerator Conference*, (2021) paper WEPAB099 (2021).
- ¹⁴B. Dunham, J. Barley, A. Bartnik, I. V. Bazarov, L. Cultrera, J. Dobbins, G. Hoffstaetter, B. Johnson, R. Kaplan, S. Karkare, V. Kostroun, Y. Li, M. Liepe, X. Liu, F. Loehl, J. M. Maxson, P. Quigley, J. Reilly, D. Rice, D. Sabol, E. Smith, K. Smolenski, M. Tigner, V. Vesherevich, D. Widger, and Z. Zhao, "Record high-average current from a high-brightness photoinjector," *Appl. Phys. Lett.* **102**, 034105 (2013).
- ¹⁵M. A. H. Schmeißer, S. Mistry, H. Kirschner, S. Schubert, A. Jankowiak, T. Kamps, and J. Kuhn, "Towards the operation of cs-k-sb photocathodes in superconducting rf photoinjectors," *Phys. Rev. Accel. Beams.* **21**, 113401 (2018).
- ¹⁶T. Vecchione, I. Ben-Zvi, D. H. Dowell, J. Feng, T. Rao, J. Smedley, W. Wan, and H. A. Padmore, "A low emittance and high efficiency vis-

This is the author's peer reviewed, accepted manuscript. However, the online version of record will be different from this version once it has been copyedited and typeset.

PLEASE CITE THIS ARTICLE AS DOI: 10.1063/5.0088306

ible light photocathode for high brightness accelerator-based x-ray light sources," *Appl. Phys. Lett.* **99**, 034103 (2011).

¹⁷L. Cultrera, S. Karkare, H. Lee, X. Liu, I. V. Bazarov, and B. Dunham, "Cold electron beams from cryocooled, alkali antimonide photocathodes," *Phys.Rev. Spec. Top.-Accel. Beams.* **18**, 113401 (2015).

¹⁸J. Feng, S. Karkare, J. Nasiatka, S. Schubert, J. Smedley, and H. A. Padmore, "Near atomically smooth alkali antimonide photocathode thin films," *J. Appl. Phys.* **121**, 044904 (2017).

¹⁹S. Karkare and I. V. Bazarov, "Effects of surface nonuniformities on the mean transverse energy from photocathodes," *Phys. Rev. App.* **4**, 024015 (2015).

²⁰G. S. Gevorkyan, S. Karkare, S. Emamian, I. V. Bazarov, and H. A. Padmore, "Effects of physical and chemical surface roughness on the brightness of electron beams from photocathodes," *Phys. Rev. Accel. Beams.* **21**, 093401 (2018).

²¹S. Schubert, M. Ruiz-Oses, I. Ben-Zvi, T. Kamps, X. Liang, E. Muller, K. Mueller, H. A. Padmore, T. Rao, X. Tong, T. Vecchione, and J. Smedley, "Bi-alkali antimonide photocathodes for high brightness accelerators," *Appl. Materials* **1**, 032119 (2013).

²²A. Galdi, J. Balajka, W. J. I. DeBenedetti, L. Cultrera, I. V. Bazarov, M. A. Hines, and J. M. Maxson, "Reduction of surface roughness emittance of cs_{3sb} photocathodes grown via codeposition on single crystal substrates," *Appl. Phys. Lett.* **118**, 244101 (2021).

²³J. T. Paul, A. Galdi, C. Parzyck, K. M. Shen, J. M. Maxson, and R. G. Hennig, "Computational synthesis of substrates by crystal cleavage," *NPJ Comput. Mater.* **7** (2021).

²⁴K. Mathew, A. K. Singh, J. J. Gabriel, K. Choudhary, S. B. Sinnott, A. V. Davydov, F. Tavazza, and R. G. Hennig, "Mpinterfases: A materials project based python tool for high-throughput computational screening of interfacial systems," *Comput. Mater. Sci.* **122** (2016).

²⁵<https://www.mtixt1.com/>.

²⁶<https://www.alfa.com/en/>.

²⁷<https://www.saesgetters.com/>.

²⁸<https://www.mbe-komponenten.de/products/mbe-components/effusion-cells.php/>.

²⁹M. Hagino and T. Takahashi, "Thickness of cs-sb films relative to the original sb films," *J. Appl. Phys.* **37**, 10 (1966).

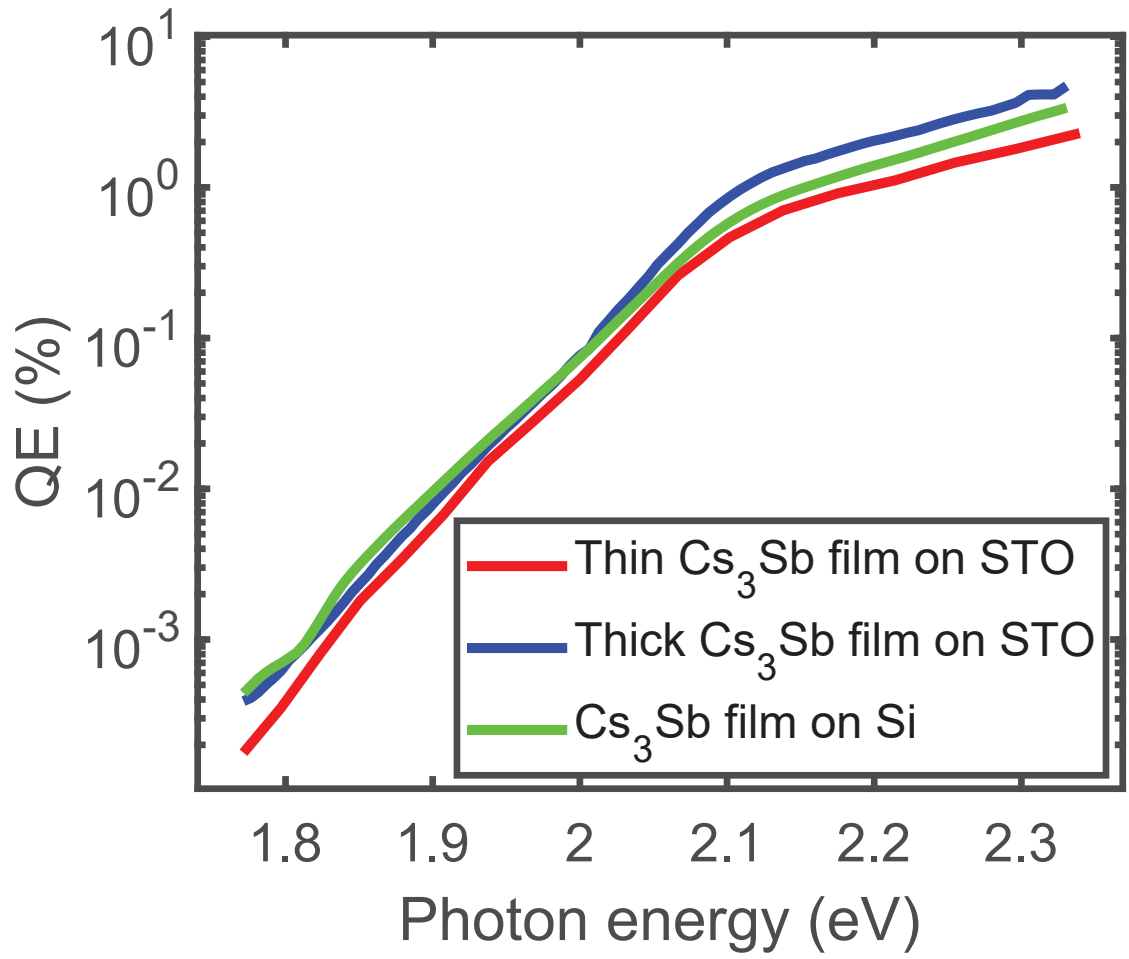
³⁰C. T. Parzyck, A. Galdi, J. K. Nangoi, W. J. I. DeBenedetti, J. Balajka, B. D. Faeth, H. Paik, C. Hu, T. A. Arias, M. A. Hines, D. G. Schlom, K. M. Shen, and J. M. Maxson, "A single-crystal alkali antimonide photocathode: high efficiency in the ultra-thin limit," (2021), arXiv:2112.14366.

³¹<https://www.budgetsensors.com/force-modulation-afm-probe-platinum-electrimum/>.

³²W. Melitz, J. Shena, A. C. Kummel, and S. Lee, "Kelvin probe force microscopy and its application," *Surface Science Reports* **66** (2011).

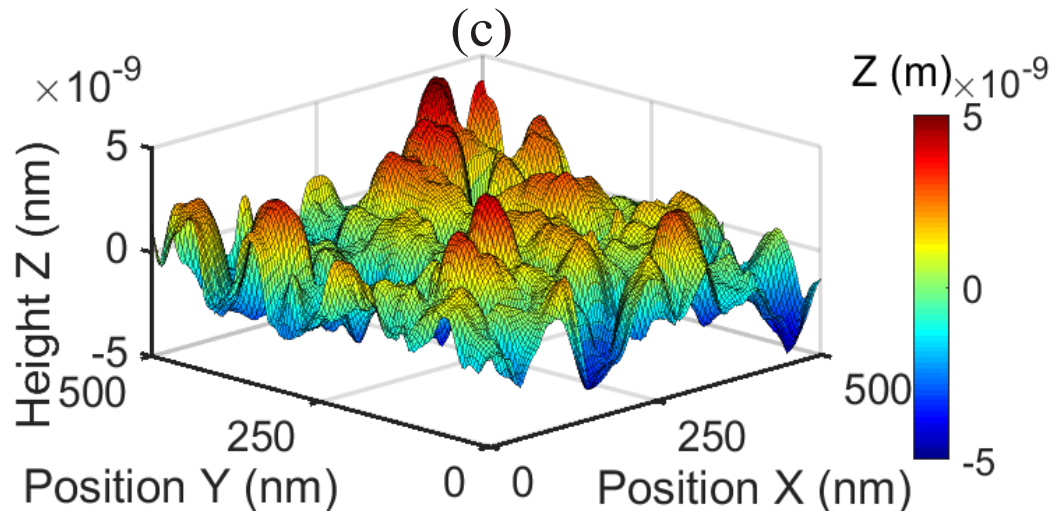
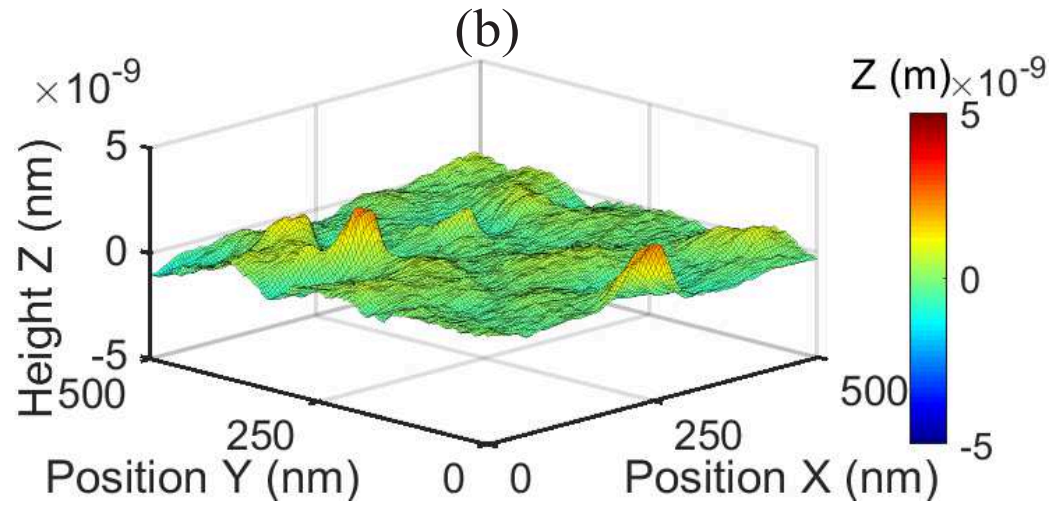
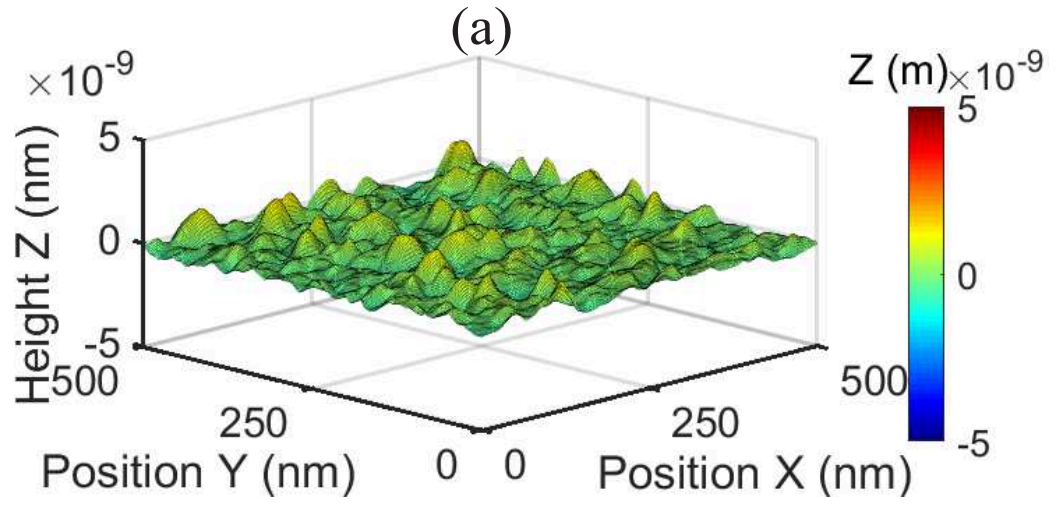
This is the author's peer reviewed, accepted manuscript. However, the online version of record will be different from this version once it has been copyedited and typeset.

PLEASE CITE THIS ARTICLE AS DOI: 10.1063/1.50088306



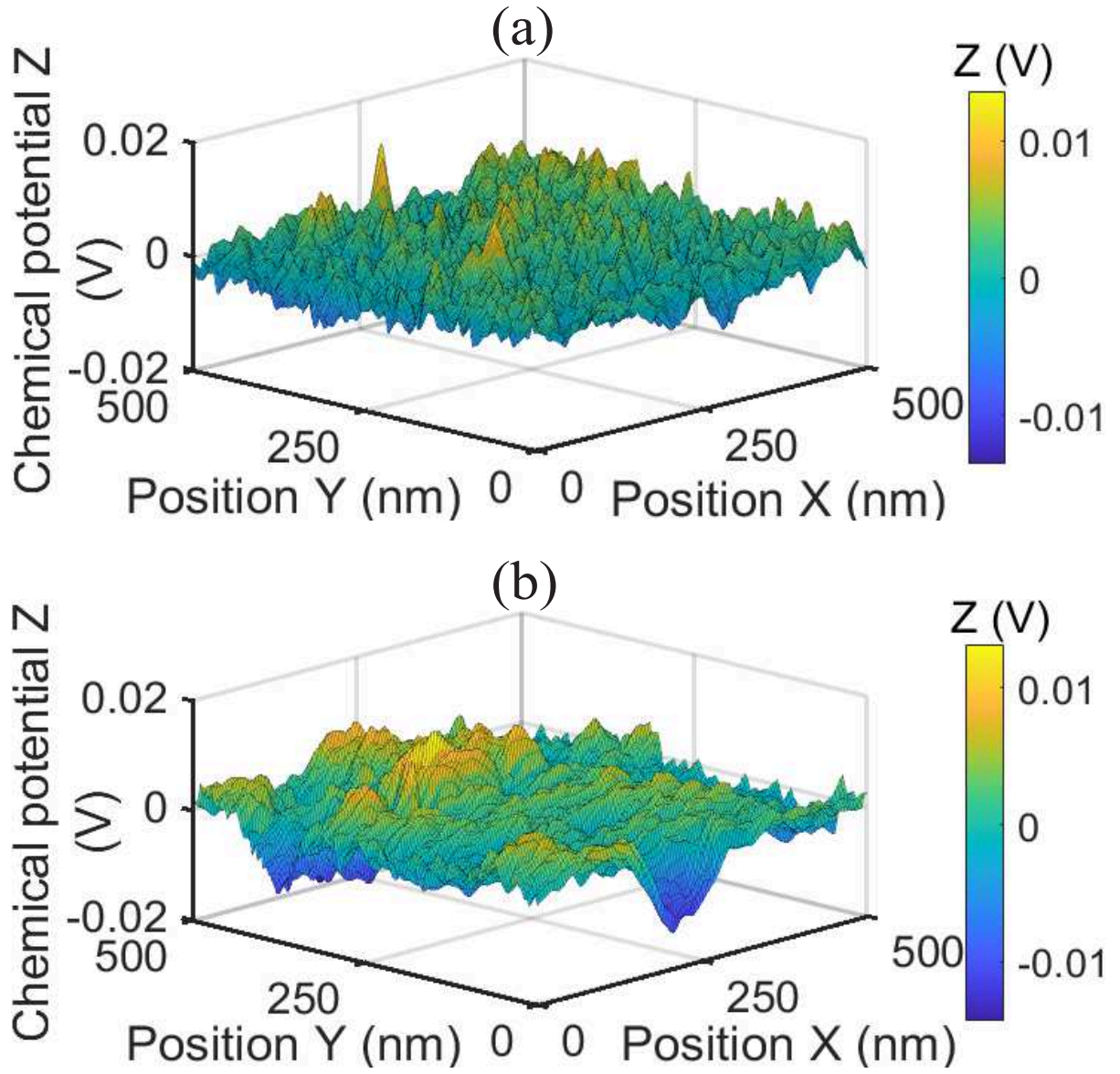
This is the author's peer reviewed, accepted manuscript. However, the online version of record will be different from this version once it has been copyedited and typeset.

PLEASE CITE THIS ARTICLE AS DOI: 10.1063/5.0088306



This is the author's peer reviewed, accepted manuscript. However, the online version of record will be different from this version once it has been copyedited and typeset.

PLEASE CITE THIS ARTICLE AS DOI: 10.1063/1.50088306



This is the author's peer reviewed, accepted manuscript. However, the online version of record will be different from this version once it has been copyedited and typeset.
PLEASE CITE THIS ARTICLE AS DOI: 10.1063/1.50088306

